A new crystalline form of β - D-lactose prepared by oven drying a concentrated aqueous solution of D-lactose

Acta Cryst C STRUCTURAL CHEMISTRY
ISSN 2053-2296

A new crystalline form of $\alpha\beta$-D-lactose prepared by oven drying a concentrated aqueous solution of D-lactose

Daniel Nicholls,[a] Carole Elleman,[b] Norman Shankland[c] and Kenneth Shankland[a]*

[a]School of Pharmacy, Whiteknights Campus, University of Reading, Reading RG6 6AD, England, [b]Reading Scientific Services Limited, Mondelez, Whiteknights Campus, Reading RG6 6LA, England, and [c]CrystallografX Limited, 2 Stewart Street, Glasgow, Strathclyde G62 6BW, Scotland. *Correspondence e-mail: k.shankland@reading.ac.uk

Received 20 May 2019
Accepted 7 June 2019

Edited by A. R. Kennedy, University of Strathclyde, Scotland

Keywords: lactose; crystal structure; powder diffraction; DFT; disaccharide; polymorph.

CCDC reference: 1921562

Supporting information: this article has supporting information at journals.iucr.org/c

A new crystalline form of $\alpha\beta$-D-lactose ($C_{12}H_{22}O_{11}$) has been prepared by the rapid drying of an approximately 40% *w*/*v* syrup of D-lactose. Initially identified from its novel powder X-ray diffraction pattern, the monoclinic crystal structure was solved from a microcrystal recovered from the generally polycrystalline mixed-phase residue obtained at the end of the drying step. This is the second crystalline form of $\alpha\beta$-D-lactose to be identified and it has a high degree of structural three-dimensional similarity to the previously identified triclinic form.

1. Introduction

D-Lactose (henceforth referred to simply as lactose) is a disaccharide that plays a very important role in the food and pharmaceutical industries (Booij, 1985; Audic *et al.*, 2003; Gohel & Jogani, 2005; Lifran *et al.*, 2000), and whose solid-state properties in both the crystalline and the amorphous states have been studied extensively for decades (Hockett & Hudson, 1931; Bushill *et al.*, 1965; Kirk *et al.*, 2007; Terban *et al.*, 2016). It exists in two anomeric forms (Fig. 1) and several crystalline forms have been reported and fully characterized crystallographically (Table 1). Methods for the preparation of the various forms have been described in considerable detail in the publications cited in Table 1 and elsewhere (Simpson *et al.*, 1982; Simone *et al.*, 2019). Whilst other forms with varying mixes of the two anomers have been reported in the literature (*e.g.* an α:β ratio of 5:3; Hockett & Hudson, 1931), these reports lack compelling crystallographic evidence to back them up. Indeed, the multidisciplinary nature of much of the research on lactose crystals and crystallization means that crystallography rarely plays the central role in the evaluation of experimental outcomes.

Our own interest in the solid-state properties of lactose stems from its significance in chocolate-crumb manufacture. Chocolate crumb is typically manufactured by the plate drying of a sweetened condensed milk (produced by either dissolving sucrose in milk or adding water to a sucrose and milk powder mixture) to ~80–90% solids. Cocoa liquor is then mixed into this material, which is subsequently dried under vacuum to leave a chocolate-crumb product (Wells, 2009). The crumb method of chocolate manufacture is widely used by larger manufacturers, in the main due to the characteristic and brand-defining flavours that crumb chocolates possess. The vacuum drying stage provides the perfect conditions for Maillard reactions to occur, allowing for the development of complex cooked flavours that can vary significantly depending

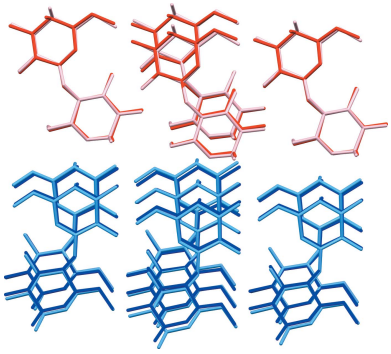

Table 1
Reported crystalline forms of D-lactose for which crystal structures are available.

Form	Abbreviation	SpGrp	Z	Z'	T (K)	Refcode	Type	Reference
α-Lactose monohydrate	α-L·H_2O	$P2_1$	2	1	150	LACTOS11	SX	Smith *et al.* (2005)
β-Lactose	β-L	$P2_1$	2	1	293	BLACTO	SX	Hirotsu & Shimada (1974)
α-Lactose (hygroscopic)	α-LH	$P2_1$	2	1	293	EYOCUQ	PXRD	Platteau *et al.* (2004)
α-Lactose (stable anhydrous)	α-LS	$P1$	2	2	293	EYOCUQ01	PXRD	Platteau *et al.* (2005)
$\alpha\beta$-lactose	$\alpha\beta$-L_T	$P1$	2	2	120	LAKKEO01	SX	Guiry *et al.* (2008)

Notes: SpGrp = space group; refcode = Cambridge Structural Database (CSD; Groom *et al.*, 2016) refcode; SX = structure determined by single-crystal X-ray diffraction; PXRD = structure determined by powder X-ray diffraction.

on the exact conditions of the drying. This dependence of flavour upon conditions means that crumb-production methodologies are often maintained secret or patented (Wells, 2009).

We have previously accurately quantified the relative proportions of crystalline and amorphous sugars in both chocolate and chocolate crumb using quantitative phase analysis (QPA) based upon powder X-ray diffraction (PXRD) (Nicholls *et al.*, 2018). Under the assumption that the majority of solid-state transformations of, and interactions between, the sugars in crumb manufacture occur during the initial plate drying of the sweetened condensed milk, we have explored the phase composition of the materials that result from drying of the somewhat simpler systems of concentrated sucrose and lactose syrups. Here, we report the results of drying syrups that contain only lactose.

2. Experimental

2.1. Sample preparation

α-Lactose monohydrate (40 g; Sigma, BN: SLBQ8461V) was dissolved in purified water (100 ml) at 45 °C on a stirring hotplate. Stirring was continued for approximately 1 h after the visual disappearance of the last dispersed solid to ensure complete dissolution. Aliquots (3 or 6 ml) were then measured out and poured into 5.5 cm Petri dishes before being placed in a Lenton Thermal Designs fan oven at a number of different temperatures (Table 2). The temperature at the level of the tray inside the oven was confirmed using an RS52 Digital Thermometer equipped with a K-type thermocouple. Preliminary experiments showed that 30 min of drying was sufficient to completely dry a 3 ml sample, but 90 min of drying was chosen for use throughout, in order to ensure complete drying of the 6 ml samples. Upon removal from the fan oven, samples were allowed to cool and the crystallized powders, which had hardened as off-white crusts in the Petri dishes, were removed using a spatula and stored in glass vials ready for analysis. Samples were lightly ground in an agate mortar and pestle in order to create free-flowing powders suitable for PXRD measurements.

Table 2
Sample drying conditions for the lactose syrups.

Sample number	Temperature (°C)	Syrup volume (ml)
1	100	3
2	100	6
3	110	3
4	110	6
5	120	3
6	120	6
7	140	3
8	140	6

2.2. Powder X-ray diffraction

Each powder was loaded into a 0.7 mm borosilicate glass capillary and mounted on a Bruker D8 Advance Diffractometer operating in transmission capillary geometry, with a LynxEye detector and monochromatic incident radiation of wavelength 1.54056 Å. Samples were typically scanned in the relatively narrow range 3–35° 2θ, with a 1 h data collection time, for phase identification purposes. All PXRD runs were performed within a few hours of the samples being removed from the oven. Data were analysed using the *EVA* (Bruker, 2018), *TOPAS* (Coelho, 2018) and *DASH* (David *et al.*, 2006) packages. PXRD data from samples of unground material, collected on a Bruker D8 operating in reflection flat plate mode, were used to verify that no phase transformations had been induced by the light grinding used in the sample preparation stage.

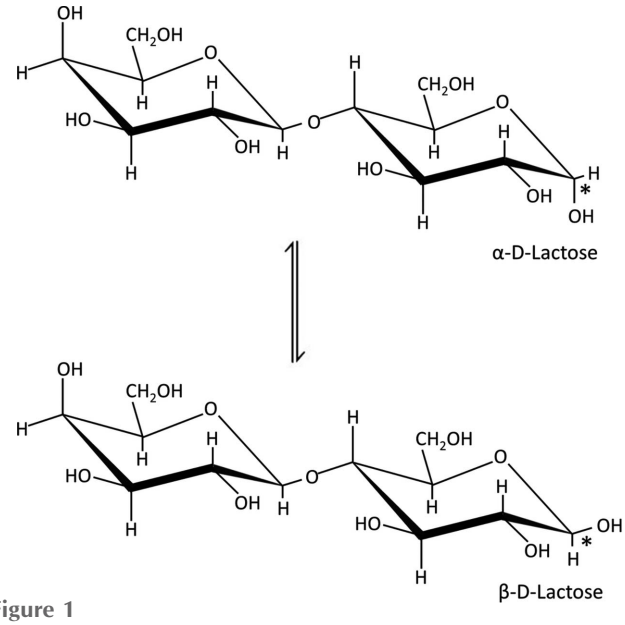

Figure 1
The molecular structures of the α and β anomers of D-lactose, with the anomeric carbon identified by an asterisk.

Table 3
Experimental details.

Crystal data	
Chemical formula	$C_{12}H_{22}O_{11}$
M_r	342.29
Crystal system, space group	Monoclinic, $P2_1$
Temperature (K)	100
a, b, c (Å)	5.0044 (3), 38.6364 (14), 7.6007 (4)
β (°)	106.200 (5)
V (Å^3)	1411.26 (13)
Z	4
Radiation type	Cu $K\alpha$
μ (mm^{-1})	1.26
Crystal size (mm)	0.08 × 0.02 × 0.02
Data collection	
Diffractometer	XtaLAB Synergy Dualflex HyPix
Absorption correction	Multi-scan (*CrysAlis PRO*; Rigaku OD, 2019)
T_{min}, T_{max}	0.804, 1.000
No. of measured, independent and observed [$I > 2\sigma(I)$] reflections	8132, 3861, 3316
R_{int}	0.057
(sin $\theta/\lambda)_{max}$ (Å^{-1})	0.597
Refinement	
$R[F^2 > 2\sigma(F^2)]$, $wR(F^2)$, S	0.048, 0.120, 1.02
No. of reflections	3861
No. of parameters	431
No. of restraints	2
H-atom treatment	H-atom parameters constrained
$\Delta\rho_{max}$, $\Delta\rho_{min}$ (e Å^{-3})	0.38, −0.25

Computer programs: *CrysAlis PRO* (Rigaku OD, 2019), *SHELXT* (Sheldrick, 2015*a*), *SHELXL2017* (Sheldrick, 2015*b*) and *OLEX2* (Dolomanov *et al.*, 2009).

2.3. Single-crystal diffraction

Dried samples were examined under a polarizing microscope to check for the possible occurrence of single crystals. Any potential single crystals were carefully removed and mounted on a Rigaku Synergy single-crystal diffractometer equipped with a microfocus copper X-ray source, a Hypix 3000 single-photon counting detector and an Oxford Cryosystems Cryostream cooling device. Atom H16 was restrained to a chemically sensible position.

2.4. Periodic density functional theory calculations

Periodic density functional theory with van der Waals dispersion corrections (DFT-D) was used for geometry optimization of the crystal structures of interest. The PBE functional was used with PAW (projector augmented wave) pseudopotentials and the Grimme D3 correction, as implemented in the *pw.x* executable of the *QuantumEspresso* program (Giannozzi *et al.*, 2009, 2017). The lengths of bonds involving H atoms were normalized using *Mercury CSD* (Macrae *et al.*, 2008) and input files for *pw.x* were then created from these normalized CIFs using the *cif2qe* script of *QuantumEspresso*. Automatic *k*-point sampling was used; the kinetic energy cut-offs for wavefunctions and charge density were 50 and 400 Ry, respectively. The convergence thresholds for total energy and forces were set at 0.0001 and 0.001 a.u., respectively. Geometry optimization was carried out in two stages, as recommended by van de Streek & Neumann (2010), with lattice parameters fixed at crystallographic values during an initial optimization and then allowed to vary in a subsequent optimization that started from the end-point of the fixed-cell calculation. All calculations were carried out on a Dell Precision T7810 workstation equipped with two 2.40 GHz 8-core Intel Xeon E5-2630 v3 CPUs, running the Microsoft *Windows 10* operating system, and using the Windows Subsystem for Linux (WSL) feature to allow the Linux-compiled MPI-enabled *pw.x* executable to utilize multiple cores.

3. Results

All of the dried samples exhibited PXRD patterns consistent with phase mixtures of crystalline lactose and, with the exception of those samples dried at 100 °C, all possessed a strong contribution from a crystalline phase that did not correspond to any of the known phases listed in Table 1 (Fig. 2). Even after identifying one of the contributing phases as β-L, attempts to index the unknown contribution(s) using *DASH* and *TOPAS* were unsuccessful. Careful examination of the 120 °C sample under a polarizing microscope revealed that whilst the bulk of the sample was obviously polycrystalline, there were also a few very small single crystals present. Single-crystal diffraction showed that most of these were β-L, but one very small (76 × 24 × 18 µm) single crystal indexed to a monoclinic cell that did not match any of the known forms. After careful Pawley refinement, to account for the ∼200 °C temperature difference between the single-crystal measurement and the PXRD experiments (see supporting information for details of the refinement approach used), it was found that this cell could explain the peak positions of the unknown phase in the PXRD pattern. A full single-crystal data collection resulted in the crystal structure of a new monoclinic form

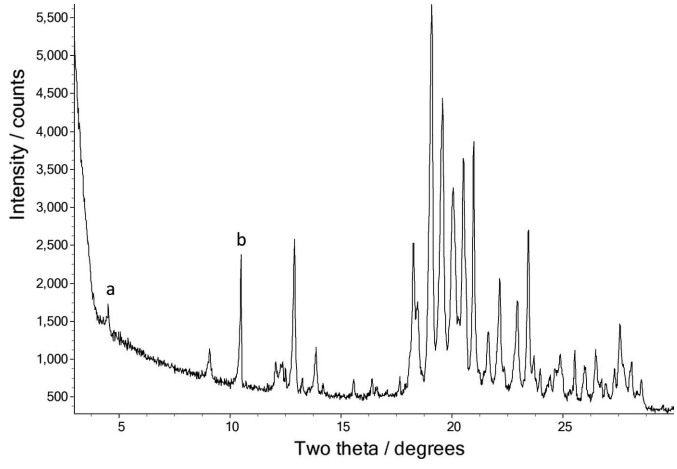

Figure 2
Powder X-ray diffraction data in the range 3–30° 2θ collected from dried sample 3. The data cannot be fully explained by the combination of any of the previously report crystal forms of lactose. The presence of β-L in the sample is evident from the diagnostic peak labelled *b*, whilst the low-angle peak labelled *a* may be attributable to α-LS, $\alpha\beta$-L$_T$ or the unknown form of lactose (subsequently identified as monoclinic $\alpha\beta$-L$_M$) that appears to comprise the bulk of the sample.

Table 4
Relative abundance of crystalline lactose phases (% *w*/*w*) in each of the samples listed in Table 2, as obtained by Rietveld-based QPA.

The estimates are approximate, since the PXRD data had not been collected with the intention of performing QPA; more accurate and precise quantification would require longer data collections over a wider 2θ range.

Sample	$\alpha\beta$-L_M	$\alpha\beta$-L_T	β-L	α-LS	α-L·H_2O
1	0	0	41	0	59
2	0	0	27	0	73
3	57	8	23	12	0
4	80	3	10	7	0
5	81	19	0	0	0
6	91	4	0	5	0
7	90	10	0	0	0
8	92	8	0	0	0

of $\alpha\beta$-D-lactose (henceforth referred to as $\alpha\beta$-L_M), whose crystallographic details are summarized in Table 3.

Knowing the structure of $\alpha\beta$-L_M, it was then possible to perform Rietveld-based QPA on the PXRD patterns in order to quantify the amounts of the various forms of crystalline lactose present in the samples (Table 4 and Fig. 3).

3.1. Discussion

Despite the small size of the crystal retrieved from the phase mixture, the crystal structure determination of $\alpha\beta$-L_M was relatively straightforward. Whilst the single-crystal diffraction data were of sufficient quality to allow the positioning of the majority of hydroxy H atoms directly from the difference Fourier maps, the location of a few such H atoms were less well determined. Geometry optimization in the solid state using DFT-D has been shown to be a powerful method for crystal structure verification (van de Streek & Neumann, 2010, 2014) and it was employed here to check the hydroxy-

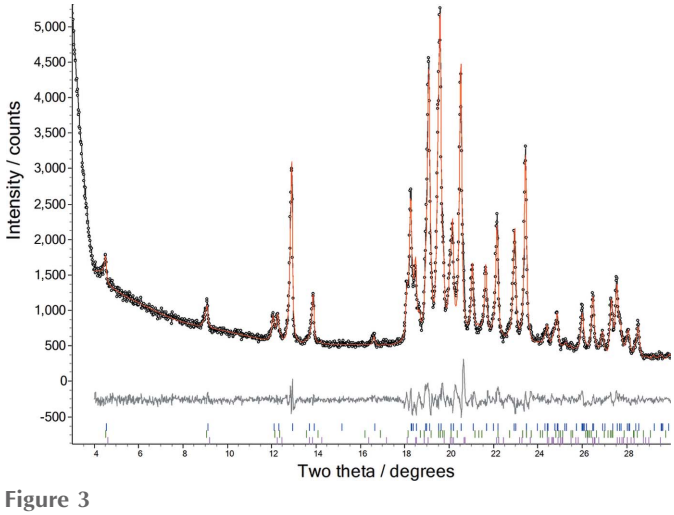

Figure 3
A three-phase Rietveld fit to the powder diffraction data in the range 3–30° 2θ collected from dried sample 6. Observed data are shown as black circles, the fit to the data is shown as a red line and the difference plot is shown in grey. Blue tick marks indicate reflection positions corresponding to $\alpha\beta$-L_M (91% *w*/*w*), green tick marks indicate reflection positions corresponding to α-LS (5% *w*/*w*) and pink tick marks indicate reflection positions corresponding to $\alpha\beta$-L_T (4% *w*/*w*).

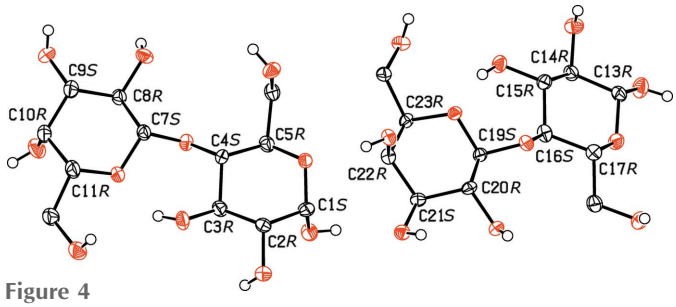

Figure 4
The contents of the asymmetric unit of the $\alpha\beta$-L_M crystal structure, with the stereochemistry of the chiral centres shown. The α anomer (left) has C1 *S*, whilst the β anomer (right) has C13 *R*.

group orientations of the single-crystal structure. Fixed-cell geometry optimization of the refined crystal structure of $\alpha\beta$-L_M gave a structure in which the position of atom H16 in particular moved significantly; specifically, 0.92 Å, corresponding to a clockwise rotation of approximately 59° around the O9—C9 bond to form a hydrogen bond [O9—H16···O11^{i}; symmetry code: (i) $x-1, y, z-1$] that was not evident in the original single-crystal structure refinement. Whilst this optimization also improved the linearity of some other hydrogen bonds (*e.g.* those involving H22, H36 and H38), only the position change of H16 was deemed to be significant enough to merit revisiting the single-crystal structure refinement. A restraint was used to hold H16 in the correct (*i.e.* DFT-D) hydrogen-bonding position in the final refinement. The asymmetric unit of the crystal structure of $\alpha\beta$-L_M, with the stereochemistry of the chiral centres highlighted, is shown in Fig. 4.

Differences between the experimental and energy-minimized $\alpha\beta$-L_M crystal structures are relatively small; a 15-molecule overlay in *Mercury* returned an r.m.s. deviation (RMSD) of 0.054 Å, a favourable value that supports the correctness of experimental $\alpha\beta$-L_M (van de Streek & Neumann, 2010). The $\alpha\beta$-L_M and $\alpha\beta$-L_T polymorphs each comprise alternating two-dimensional layers of α and β anomers (Fig. 5), and $\alpha\beta$-L_M shows a high degree of three-dimensional similarity with $\alpha\beta$-L_T (Fig. 6 and supporting information). Unsurprisingly, the DFT-D total energy difference between the asymmetric units of the polymorphs is too small to infer the rank order of stability: $\Delta E_{(\alpha\beta\text{-}L_M-\alpha\beta\text{-}L_T)}$ = 1.8 kJ mol^{-1}, with the energy for $\alpha\beta$-L_T calculated using the corrected and energy-minimized $\alpha\beta$-L_T crystal structure of van de Streek & Neumann (2014).

The use of PXRD was crucial in identifying the presence of a new crystalline form of lactose. However, the complexity of the phase mixtures returned in the crystallizations, coupled with the relatively large unit cell size of $\alpha\beta$-L_M, meant that we were unable to index it from the PXRD alone.

Appearing to comprise the bulk of the material recovered from crystallizations occurring at temperatures of 110 °C or above, the $\alpha\beta$-L_M phase was clearly polycrystalline in nature; from all the samples prepared, only one very small crystal of $\alpha\beta$-L_M suitable for single-crystal diffraction was ever recovered. In spite of its diminutive size, the crystal diffracted sufficiently well to yield a crystal structure that, as evidenced

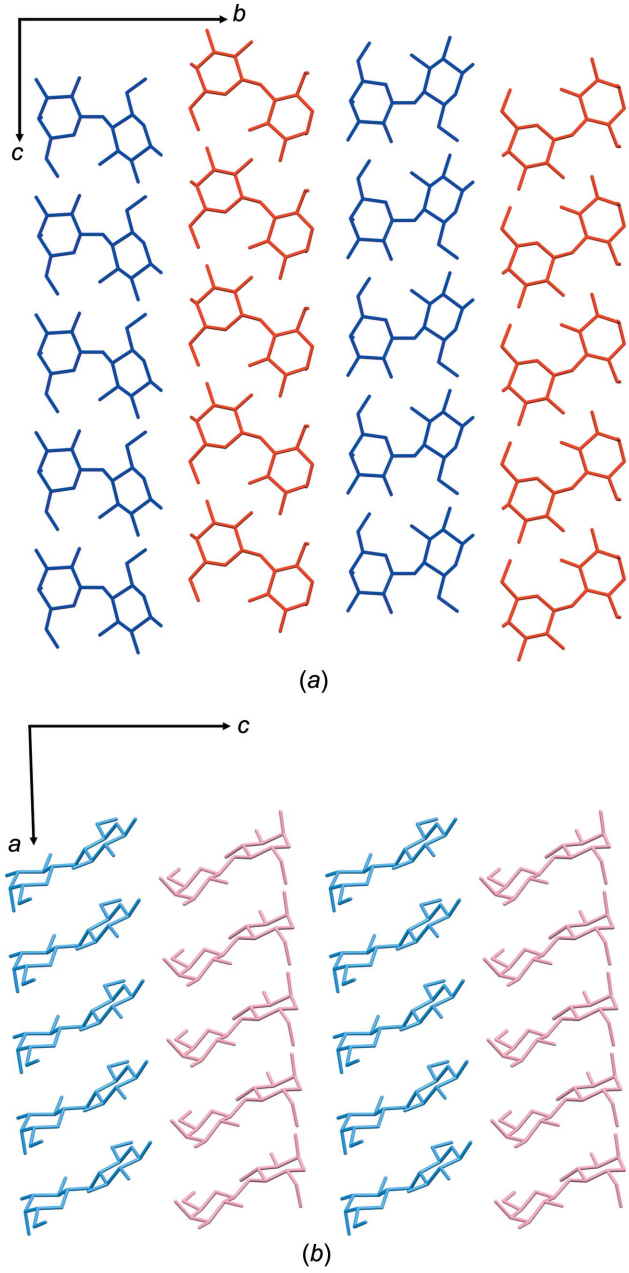

Figure 5
Packing diagrams of (*a*) $\alpha\beta$-L_M and (*b*) $\alpha\beta$-L_T. Both crystal structures comprise alternating two-dimensional layers of the α (red, salmon) and β anomers (blue, light blue).

by Rietveld-based QPA, proved to constitute the majority phase in bulk samples 3 to 8. Whilst we did not attempt any quantification of the amorphous content, the relatively low backgrounds of all the collected PXRD data sets suggest that there is little in the way of amorphous material in the recrystallized samples and we observed no changes in the PXRD of samples as a function of time over a timescale of 12 months.

The QPA analysis shows that the composition of the phase mixtures returned from the syrup-drying experiments exhibit a temperature dependence. It also shows clearly that the previously identified form $\alpha\beta$-L_T crystallizes alongside $\alpha\beta$-L_M

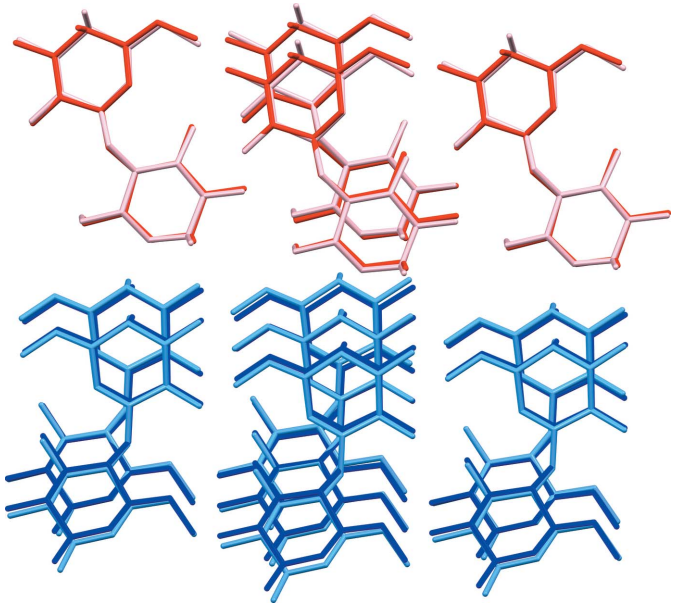

Figure 6
The three-dimensional similarity of $\alpha\beta$-L_M and $\alpha\beta$-L_T, illustrated by overlaying molecules in each structure using the 'Crystal Packing Similarity' feature of *Mercury* (Macrae *et al.*, 2008). The RMSD for the overlay is 0.336 Å and the colour coding used is the same as in Fig. 5.

in the syrup-drying process, adding to the existing methods of Lefebvre *et al.* (2005) and Guiry *et al.* (2008) for the crystallization of $\alpha\beta$-L_T.

4. Conclusion

The use of PXRD, single-crystal diffraction and periodic DFT-D has allowed the identification and structure determination of a new monoclinic crystalline form of $\alpha\beta$-D-lactose. The structure adds to the five known well-characterized forms of D-lactose. Many recent publications (Fan & Roos, 2015; Haque & Roos, 2005; Jouppila *et al.*, 1998; Nijdam *et al.*, 2007; Saffari *et al.*, 2015; Yazdanpanah & Langrish, 2011) continue to cite literature whose lactose phase identification methods are sub-optimal (*i.e.* based upon tabulated PXRD line positions and estimated intensities), and which continue to refer to mixed phase forms (such as α:β = 5:3 and α:β = 4:1) that lack compelling crystallographic evidence for their existence. It is recommended that where PXRD is to play a role in phase identification in lactose mixtures, the analysis should be based on whole-pattern fitting methods using verified crystal structures, and ideally employ transmission (as opposed to the more widely used reflection) instrument geometry, in order to minimize the confounding effects of preferred orientation in samples.

Acknowledgements

The authors acknowledge the University of Reading's Chemical Analysis Facility for X-ray diffraction facilities and thank Mr Nick Spencer for his technical support of those facilities

Funding information

Funding for this research was provided by: Biotechnology and Biological Sciences Research Council (BBSRC) and Mondelez Ltd (Case Award BB/L015730/1, to DN).

References

Audic, J.-L., Chaufer, B. & Daufin, G. (2003). *Lait*, **83**, 417–438.
Booij, C. J. (1985). *Int. J. Dairy Technol.* **38**, 105–109.
Bruker (2018). *EVA*. Bruker AXS Inc., Madison, Wisconsin, USA. https://www.bruker.com/products/x-ray-diffraction-and-elemental-analysis/x-ray-diffraction/xrd-software/eva/overview.html.
Bushill, J. H., Wright, W. B., Fuller, C. H. F. & Bell, A. V. (1965). *J. Sci. Food Agric.* **16**, 622–628.
Coelho, A. A. (2018). *J. Appl. Cryst.* **51**, 210–218.
David, W. I. F., Shankland, K., van de Streek, J., Pidcock, E., Motherwell, W. D. S. & Cole, J. C. (2006). *J. Appl. Cryst.* **39**, 910–915.
Dolomanov, O. V., Bourhis, L. J., Gildea, R. J., Howard, J. A. K. & Puschmann, H. (2009). *J. Appl. Cryst.* **42**, 339–341.
Fan, F. H. & Roos, Y. H. (2015). *Food. Res. Int.* **67**, 1–11.
Giannozzi, P., *et al.* (2017). *J. Phys. Condens. Matter*, **29**, article No. 465901.
Giannozzi, P., *et al.* (2009). *J. Phys. Condens. Matter*, **21**, article No. 395502.
Gohel, M. C. J. P. D. & Jogani, P. D. (2005). *J. Pharm. Pharm. Sci.* **8**, 76–93.
Groom, C. R., Bruno, I. J., Lightfoot, M. P. & Ward, S. C. (2016). *Acta Cryst.* B**72**, 171–179.
Guiry, K. P., Coles, S. J., Moynihan, H. A. & Lawrence, S. E. (2008). *Cryst. Growth Des.* **8**, 3927–3934.
Haque, K. & Roos, Y. H. (2005). *Carbohydr. Res.* **340**, 293–301.
Hirotsu, K. & Shimada, A. (1974). *Bull. Chem. Soc. Jpn*, **47**, 1872–1879.
Hockett, R. C. & Hudson, C. S. (1931). *J. Am. Chem. Soc.* **53**, 4455–4456.
Jouppila, K., Kansikas, J. & Roos, Y. H. (1998). *Biotechnol. Prog.* **14**, 347–350.
Kirk, J. H., Dann, S. E. & Blatchford, C. G. (2007). *Int. J. Pharm.* **334**, 103–114.
Lefebvre, J., Willart, J.-F., Caron, V., Lefort, R., Affouard, F. & Danède, F. (2005). *Acta Cryst.* B**61**, 455–463.
Lifran, E. V., Hourigan, J. A., Sleigh, R. W. & Johnson, R. L. (2000). *Food Aust.* **52**, 120–136.
Macrae, C. F., Bruno, I. J., Chisholm, J. A., Edgington, P. R., McCabe, P., Pidcock, E., Rodriguez-Monge, L., Taylor, R., van de Streek, J. & Wood, P. A. (2008). *J. Appl. Cryst.* **41**, 466–470.
Nicholls, D., Shankland, K., Spillman, M. & Elleman, C. (2018). *Food Anal. Methods*, **11**, 2673–2681.
Nijdam, J., Ibach, A., Eichhorn, K. & Kind, M. (2007). *Carbohydr. Res.* **342**, 2354–2364.
Platteau, C., Lefebvre, J., Affouard, F. & Derollez, P. (2004). *Acta Cryst.* B**60**, 453–460.
Platteau, C., Lefebvre, J., Affouard, F., Willart, J.-F., Derollez, P. & Mallet, F. (2005). *Acta Cryst.* B**61**, 185–191.
Rigaku OD (2019). *CrysAlis PRO*. Rigaku Oxford Diffraction Ltd, Yarnton, Oxfordshire, England.
Saffari, M., Ebrahimi, A. & Langrish, T. (2015). *J. Food Eng.* **164**, 1–9.
Sheldrick, G. M. (2015*a*). *Acta Cryst.* A**71**, 3–8.
Sheldrick, G. M. (2015*b*). *Acta Cryst.* C**71**, 3–8.
Simone, E., Tyler, A. I. I., Kuah, D., Bao, X. F., Ries, M. E. & Baker, D. (2019). *Org. Process Res. Dev.* **23**, 220–233.
Simpson, T. D., Parrish, F. W. & Nelson, M. L. (1982). *J. Food Sci.* **47**, 1948–1951.
Smith, J. H., Dann, S. E., Elsegood, M. R. J., Dale, S. H. & Blatchford, C. G. (2005). *Acta Cryst.* E**61**, o2499–o2501.
Streek, J. van de & Neumann, M. A. (2010). *Acta Cryst.* B**66**, 544–558.
Streek, J. van de & Neumann, M. A. (2014). *Acta Cryst.* B**70**, 1020–1032.
Terban, M. W., Cheung, E. Y., Krolikowski, P. & Billinge, S. J. L. (2016). *Cryst. Growth Des.* **16**, 210–220.
Wells, M. A. (2009). In *Beckett's Industrial Chocolate Manufacture and Use*, edited by S. Beckett. UK: Wiley–Blackwell.
Yazdanpanah, N. & Langrish, T. A. G. (2011). *Drying Technol.* **29**, 1046–1057.

supporting information

Acta Cryst. (2019). C**75**, 904-909 [https://doi.org/10.1107/S2053229619008210]

A new crystalline form of *αβ*-D-lactose prepared by oven drying a concentrated aqueous solution of D-lactose

Daniel Nicholls, Carole Elleman, Norman Shankland and Kenneth Shankland

Computing details

Data collection: *CrysAlis PRO* (Rigaku OD, 2019); cell refinement: *CrysAlis PRO* (Rigaku OD, 2019); data reduction: *CrysAlis PRO* (Rigaku OD, 2019); program(s) used to solve structure: SHELXT (Sheldrick, 2015a); program(s) used to refine structure: *SHELXL2017* (Sheldrick, 2015b); molecular graphics: OLEX2 (Dolomanov *et al.*, 2009); software used to prepare material for publication: OLEX2 (Dolomanov *et al.*, 2009).

αβ-D-Lactose

Crystal data

$C_{12}H_{22}O_{11}$
M_r = 342.29
Monoclinic, $P2_1$
a = 5.0044 (3) Å
b = 38.6364 (14) Å
c = 7.6007 (4) Å
β = 106.200 (5)°
V = 1411.26 (13) Å^3
Z = 4
$F(000)$ = 728
D_x = 1.611 Mg m^{-3}
Cu $K\alpha$ radiation, λ = 1.54184 Å
Cell parameters from 3068 reflections
θ = 4.5–72.2°
μ = 1.26 mm^{-1}
T = 100 K
Clear block, colourless
0.08 × 0.02 × 0.02 mm

Data collection

XtaLAB Synergy Dualflex HyPix diffractometer
Radiation source: micro-focus sealed X-ray tube, PhotonJet (Cu) X-ray Source
Mirror monochromator
Detector resolution: 10.0000 pixels mm^{-1}
ω scans
Absorption correction: multi-scan (CrysAlis PRO; Rigaku OD, 2019)
T_{min} = 0.804, T_{max} = 1.000
8132 measured reflections
3861 independent reflections
3316 reflections with $I > 2\sigma(I)$
R_{int} = 0.057
θ_{max} = 67.1°, θ_{min} = 4.6°
h = −5→5
k = −46→41
l = −8→9

Refinement

Refinement on F^2
Least-squares matrix: full
$R[F^2 > 2\sigma(F^2)]$ = 0.048
$wR(F^2)$ = 0.120
S = 1.01
3861 reflections
431 parameters
2 restraints
Primary atom site location: dual
Hydrogen site location: inferred from neighbouring sites
H-atom parameters constrained
$w = 1/[\sigma^2(F_o^2) + (0.0705P)^2]$ where $P = (F_o^2 + 2F_c^2)/3$
$(\Delta/\sigma)_{max} < 0.001$
$\Delta\rho_{max}$ = 0.38 e Å^{-3}
$\Delta\rho_{min}$ = −0.25 e Å^{-3}

Absolute structure: Flack *x* determined using 989 quotients [(I+)-(I-)]/[(I+)+(I-)] (Parsons *et al.*, 2013)
Absolute structure parameter: −0.3 (2)

Special details

Geometry. All esds (except the esd in the dihedral angle between two l.s. planes) are estimated using the full covariance matrix. The cell esds are taken into account individually in the estimation of esds in distances, angles and torsion angles; correlations between esds in cell parameters are only used when they are defined by crystal symmetry. An approximate (isotropic) treatment of cell esds is used for estimating esds involving l.s. planes.

Fractional atomic coordinates and isotropic or equivalent isotropic displacement parameters (Å²)

	x	*y*	*z*	U_{iso}*/U_{eq}
O15	1.0019 (7)	0.63348 (8)	0.4404 (5)	0.0179 (7)
O5	0.2846 (7)	0.46940 (8)	0.5118 (5)	0.0194 (7)
O18	0.7775 (7)	0.58691 (8)	0.2858 (5)	0.0169 (7)
O19	1.1446 (7)	0.59577 (9)	0.7705 (5)	0.0205 (8)
H36	1.070821	0.602565	0.847849	0.031*
O4	0.2455 (7)	0.38585 (9)	0.2851 (5)	0.0200 (7)
O21	0.4712 (7)	0.53444 (8)	0.4336 (5)	0.0184 (7)
H40	0.418775	0.516359	0.469732	0.028*
O2	0.5130 (8)	0.41768 (9)	0.9313 (5)	0.0223 (8)
H4	0.620665	0.402031	0.924954	0.034*
O22	0.6082 (7)	0.56071 (10)	−0.0652 (5)	0.0231 (8)
H44	0.466259	0.570697	−0.123045	0.035*
O8	−0.0739 (8)	0.37157 (9)	−0.0756 (5)	0.0232 (8)
H14	−0.012004	0.371203	−0.164754	0.035*
O6	−0.1588 (7)	0.46187 (10)	0.1878 (5)	0.0249 (8)
H11	−0.258564	0.452202	0.097042	0.037*
O1	0.7333 (7)	0.45878 (9)	0.7036 (5)	0.0246 (8)
H2	0.797135	0.478314	0.703099	0.037*
O17	1.5575 (8)	0.70155 (9)	0.7603 (5)	0.0248 (8)
H33	1.429173	0.705620	0.804827	0.037*
O16	1.4840 (8)	0.69894 (9)	0.3686 (5)	0.0238 (8)
O20	0.9133 (7)	0.52636 (9)	0.7562 (5)	0.0208 (7)
H38	0.846224	0.539715	0.816208	0.031*
O13	1.1060 (8)	0.68991 (10)	−0.1138 (5)	0.0258 (8)
H26	0.944059	0.695554	−0.125458	0.039*
O12	1.5346 (9)	0.72657 (10)	0.1161 (6)	0.0299 (9)
H24	1.586499	0.744594	0.172184	0.045*
O3	0.2259 (8)	0.36874 (9)	0.6726 (5)	0.0257 (8)
H6	0.244093	0.351721	0.612530	0.039*
O11	0.2818 (9)	0.28643 (10)	0.6678 (5)	0.0315 (9)
H22	0.150035	0.298206	0.677066	0.047*
O9	−0.1599 (8)	0.30041 (10)	−0.1734 (5)	0.0271 (8)
H16	−0.315580	0.306148	−0.235115	0.041*
O7	0.2127 (8)	0.32976 (9)	0.3684 (5)	0.0246 (8)
O14	0.9488 (8)	0.62845 (9)	0.0366 (5)	0.0243 (8)

H28	0.880367	0.614191	0.091229	0.036*
O10	0.2774 (9)	0.27554 (10)	0.1138 (6)	0.0330 (9)
H18	0.314497	0.255156	0.139478	0.050*
C20	0.9358 (10)	0.58351 (13)	0.6136 (7)	0.0181 (10)
H35	0.750213	0.590714	0.618473	0.022*
C8	0.0534 (11)	0.34525 (13)	0.0480 (8)	0.0205 (11)
H13	0.239621	0.340667	0.035068	0.025*
C24	0.5550 (11)	0.54250 (13)	0.0855 (7)	0.0198 (11)
H42	0.546449	0.517815	0.061304	0.024*
H43	0.377551	0.549730	0.101453	0.024*
C1	0.4517 (10)	0.46096 (14)	0.6919 (7)	0.0213 (11)
H1	0.426733	0.479139	0.775768	0.026*
C23	0.7860 (10)	0.55020 (12)	0.2579 (7)	0.0173 (10)
H41	0.965279	0.544004	0.238128	0.021*
C21	0.9528 (10)	0.54400 (12)	0.6007 (7)	0.0173 (10)
H37	1.140872	0.538424	0.594368	0.021*
C19	0.9984 (10)	0.59750 (12)	0.4411 (7)	0.0170 (10)
H34	1.176610	0.588406	0.431537	0.020*
C6	0.1254 (11)	0.45800 (13)	0.1900 (8)	0.0226 (11)
H9	0.198228	0.480200	0.165561	0.027*
H10	0.138072	0.442088	0.093988	0.027*
C14	1.2288 (11)	0.67893 (13)	0.0680 (7)	0.0209 (11)
H25	1.387599	0.664168	0.066897	0.025*
C17	1.3112 (10)	0.68082 (13)	0.4579 (7)	0.0195 (10)
H30	1.159935	0.696013	0.468979	0.023*
C7	0.0784 (11)	0.35677 (13)	0.2441 (7)	0.0196 (10)
H12	−0.106122	0.361692	0.259024	0.024*
C5	0.3006 (11)	0.44434 (13)	0.3749 (7)	0.0219 (11)
H8	0.494524	0.442104	0.372289	0.026*
C3	0.3540 (11)	0.39801 (13)	0.6144 (7)	0.0218 (11)
H5	0.546689	0.392342	0.619038	0.026*
C13	1.3417 (11)	0.71003 (13)	0.1898 (7)	0.0215 (11)
H23	1.190363	0.725882	0.193211	0.026*
C15	1.0364 (11)	0.65786 (13)	0.1498 (7)	0.0202 (10)
H27	0.872987	0.671902	0.148950	0.024*
C22	0.7497 (10)	0.53044 (13)	0.4241 (7)	0.0170 (10)
H39	0.786548	0.505824	0.410362	0.020*
C2	0.3514 (11)	0.42673 (13)	0.7521 (7)	0.0187 (10)
H3	0.158699	0.429934	0.755627	0.022*
C4	0.1963 (11)	0.40929 (13)	0.4195 (7)	0.0195 (11)
H7	−0.003568	0.410561	0.407681	0.023*
C18	1.4912 (11)	0.67173 (14)	0.6449 (7)	0.0234 (11)
H31	1.395514	0.654941	0.700426	0.028*
H32	1.661968	0.661189	0.634382	0.028*
C16	1.1883 (11)	0.64855 (13)	0.3472 (7)	0.0208 (11)
H29	1.338142	0.632143	0.348393	0.025*
C9	−0.1179 (12)	0.31185 (14)	0.0111 (8)	0.0249 (11)
H15	−0.300892	0.316837	0.028450	0.030*

C10	0.0178 (12)	0.28397 (13)	0.1469 (8)	0.0268 (12)
H17	−0.101628	0.263421	0.128141	0.032*
C11	0.0587 (13)	0.29805 (13)	0.3428 (8)	0.0286 (12)
H19	−0.123605	0.302114	0.363263	0.034*
C12	0.2247 (14)	0.27321 (15)	0.4875 (8)	0.0317 (13)
H20	0.121673	0.251740	0.480278	0.038*
H21	0.399212	0.267975	0.461291	0.038*

Atomic displacement parameters (Å²)

	U^{11}	U^{22}	U^{33}	U^{12}	U^{13}	U^{23}
O15	0.0173 (17)	0.0172 (16)	0.0209 (18)	−0.0002 (13)	0.0082 (13)	0.0022 (14)
O5	0.0161 (17)	0.0164 (16)	0.024 (2)	0.0003 (13)	0.0020 (14)	−0.0004 (14)
O18	0.0148 (17)	0.0183 (17)	0.0165 (17)	−0.0005 (13)	0.0025 (13)	−0.0011 (14)
O19	0.0222 (19)	0.0210 (17)	0.0166 (18)	−0.0009 (14)	0.0025 (14)	−0.0026 (14)
O4	0.0201 (18)	0.0174 (16)	0.0233 (19)	−0.0019 (14)	0.0077 (14)	−0.0017 (15)
O21	0.0125 (17)	0.0173 (17)	0.027 (2)	−0.0005 (13)	0.0073 (14)	0.0017 (15)
O2	0.023 (2)	0.0237 (19)	0.0196 (19)	0.0007 (14)	0.0043 (15)	0.0013 (15)
O22	0.0196 (17)	0.029 (2)	0.0198 (19)	0.0023 (15)	0.0045 (14)	0.0028 (15)
O8	0.029 (2)	0.0233 (18)	0.0177 (19)	0.0052 (15)	0.0074 (15)	0.0051 (16)
O6	0.0172 (18)	0.029 (2)	0.026 (2)	0.0030 (15)	0.0012 (14)	−0.0057 (16)
O1	0.0186 (18)	0.0229 (18)	0.032 (2)	−0.0011 (14)	0.0059 (15)	0.0012 (17)
O17	0.026 (2)	0.0273 (19)	0.023 (2)	−0.0052 (15)	0.0090 (15)	−0.0036 (16)
O16	0.0262 (19)	0.0230 (19)	0.0212 (19)	−0.0078 (15)	0.0049 (15)	0.0014 (15)
O20	0.0215 (19)	0.0214 (17)	0.0195 (19)	0.0002 (14)	0.0058 (14)	0.0007 (15)
O13	0.0216 (19)	0.032 (2)	0.0235 (19)	−0.0018 (16)	0.0056 (15)	0.0026 (16)
O12	0.035 (2)	0.025 (2)	0.031 (2)	−0.0097 (17)	0.0120 (18)	−0.0032 (17)
O3	0.040 (2)	0.0153 (16)	0.024 (2)	−0.0033 (16)	0.0128 (17)	−0.0002 (15)
O11	0.044 (3)	0.026 (2)	0.025 (2)	0.0022 (17)	0.0102 (18)	0.0042 (17)
O9	0.029 (2)	0.028 (2)	0.0200 (19)	−0.0021 (16)	0.0000 (15)	−0.0044 (16)
O7	0.034 (2)	0.0160 (17)	0.021 (2)	−0.0001 (15)	0.0030 (15)	0.0012 (15)
O14	0.030 (2)	0.0206 (18)	0.023 (2)	−0.0083 (15)	0.0076 (15)	−0.0009 (15)
O10	0.043 (2)	0.0229 (18)	0.034 (2)	0.0112 (17)	0.0104 (18)	0.0000 (17)
C20	0.014 (2)	0.022 (2)	0.016 (2)	−0.0002 (19)	0.0009 (18)	−0.002 (2)
C8	0.020 (3)	0.018 (2)	0.023 (3)	−0.0012 (19)	0.005 (2)	0.001 (2)
C24	0.018 (3)	0.019 (2)	0.021 (3)	0.0002 (18)	0.002 (2)	0.001 (2)
C1	0.013 (2)	0.024 (3)	0.024 (3)	−0.001 (2)	0.000 (2)	0.001 (2)
C23	0.015 (2)	0.019 (2)	0.018 (2)	0.0020 (19)	0.0045 (18)	−0.005 (2)
C21	0.014 (2)	0.021 (3)	0.017 (2)	0.0005 (18)	0.0042 (18)	0.001 (2)
C19	0.017 (3)	0.017 (2)	0.017 (2)	0.0024 (18)	0.0035 (19)	−0.0022 (19)
C6	0.023 (3)	0.020 (2)	0.027 (3)	0.001 (2)	0.010 (2)	0.000 (2)
C14	0.024 (3)	0.018 (2)	0.021 (3)	0.000 (2)	0.007 (2)	0.002 (2)
C17	0.019 (3)	0.022 (3)	0.020 (3)	−0.0018 (19)	0.0090 (19)	0.001 (2)
C7	0.023 (3)	0.016 (2)	0.020 (3)	−0.002 (2)	0.007 (2)	0.001 (2)
C5	0.017 (3)	0.019 (2)	0.029 (3)	0.001 (2)	0.004 (2)	0.002 (2)
C3	0.026 (3)	0.019 (2)	0.022 (3)	0.003 (2)	0.007 (2)	0.001 (2)
C13	0.027 (3)	0.018 (2)	0.020 (3)	−0.001 (2)	0.007 (2)	0.004 (2)
C15	0.022 (3)	0.020 (2)	0.018 (3)	0.001 (2)	0.006 (2)	−0.002 (2)

C22	0.011 (2)	0.018 (2)	0.024 (3)	0.0000 (18)	0.0084 (19)	0.000 (2)
C2	0.016 (3)	0.020 (2)	0.020 (3)	0.0027 (19)	0.0052 (19)	0.002 (2)
C4	0.022 (3)	0.016 (2)	0.018 (3)	−0.0006 (19)	0.0025 (19)	−0.003 (2)
C18	0.025 (3)	0.021 (2)	0.025 (3)	−0.003 (2)	0.008 (2)	0.003 (2)
C16	0.019 (3)	0.019 (2)	0.027 (3)	−0.001 (2)	0.011 (2)	0.001 (2)
C9	0.029 (3)	0.020 (2)	0.025 (3)	−0.001 (2)	0.007 (2)	−0.003 (2)
C10	0.038 (3)	0.017 (3)	0.024 (3)	−0.002 (2)	0.007 (2)	−0.002 (2)
C11	0.043 (3)	0.018 (3)	0.024 (3)	−0.003 (2)	0.009 (2)	0.002 (2)
C12	0.049 (4)	0.023 (3)	0.021 (3)	0.003 (3)	0.007 (2)	0.001 (2)

Geometric parameters (Å, º)

O15—C19	1.390 (6)	C20—C19	1.529 (7)
O15—C16	1.443 (6)	C8—H13	0.9800
O5—C1	1.428 (6)	C8—C7	1.527 (8)
O5—C5	1.440 (6)	C8—C9	1.531 (7)
O18—C23	1.437 (6)	C24—H42	0.9700
O18—C19	1.433 (6)	C24—H43	0.9700
O19—H36	0.8200	C24—C23	1.515 (7)
O19—C20	1.429 (6)	C1—H1	0.9800
O4—C7	1.383 (6)	C1—C2	1.529 (7)
O4—C4	1.437 (6)	C23—H41	0.9800
O21—H40	0.8200	C23—C22	1.530 (7)
O21—C22	1.424 (6)	C21—H37	0.9800
O2—H4	0.8200	C21—C22	1.532 (7)
O2—C2	1.420 (7)	C19—H34	0.9800
O22—H44	0.8200	C6—H9	0.9700
O22—C24	1.432 (6)	C6—H10	0.9700
O8—H14	0.8200	C6—C5	1.528 (8)
O8—C8	1.410 (6)	C14—H25	0.9800
O6—H11	0.8200	C14—C13	1.526 (7)
O6—C6	1.426 (6)	C14—C15	1.520 (7)
O1—H2	0.8200	C17—H30	0.9800
O1—C1	1.390 (6)	C17—C18	1.497 (7)
O17—H33	0.8200	C17—C16	1.533 (7)
O17—C18	1.430 (7)	C7—H12	0.9800
O16—C17	1.423 (6)	C5—H8	0.9800
O16—C13	1.414 (7)	C5—C4	1.523 (7)
O20—H38	0.8200	C3—H5	0.9800
O20—C21	1.425 (6)	C3—C2	1.528 (7)
O13—H26	0.8200	C3—C4	1.535 (7)
O13—C14	1.411 (7)	C13—H23	0.9800
O12—H24	0.8200	C15—H27	0.9800
O12—C13	1.399 (7)	C15—C16	1.524 (8)
O3—H6	0.8200	C22—H39	0.9800
O3—C3	1.429 (7)	C2—H3	0.9800
O11—H22	0.8200	C4—H7	0.9800
O11—C12	1.415 (7)	C18—H31	0.9700

O9—H16	0.8200	C18—H32	0.9700
O9—C9	1.429 (7)	C16—H29	0.9800
O7—C7	1.442 (6)	C9—H15	0.9800
O7—C11	1.432 (7)	C9—C10	1.515 (8)
O14—H28	0.8200	C10—H17	0.9800
O14—C15	1.419 (6)	C10—C11	1.544 (8)
O10—H18	0.8200	C11—H19	0.9800
O10—C10	1.428 (7)	C11—C12	1.520 (8)
C20—H35	0.9800	C12—H20	0.9700
C20—C21	1.534 (7)	C12—H21	0.9700

C19—O15—C16	114.6 (4)	O4—C7—C8	109.7 (4)
C1—O5—C5	113.8 (4)	O4—C7—H12	110.3
C19—O18—C23	110.8 (3)	O7—C7—C8	108.9 (4)
C20—O19—H36	109.5	O7—C7—H12	110.3
C7—O4—C4	117.3 (4)	C8—C7—H12	110.3
C22—O21—H40	109.5	O5—C5—C6	107.4 (4)
C2—O2—H4	109.5	O5—C5—H8	109.2
C24—O22—H44	109.5	O5—C5—C4	110.2 (4)
C8—O8—H14	109.5	C6—C5—H8	109.2
C6—O6—H11	109.5	C4—C5—C6	111.6 (4)
C1—O1—H2	109.5	C4—C5—H8	109.2
C18—O17—H33	109.5	O3—C3—H5	109.5
C13—O16—C17	113.4 (4)	O3—C3—C2	105.8 (4)
C21—O20—H38	109.5	O3—C3—C4	111.7 (4)
C14—O13—H26	109.5	C2—C3—H5	109.5
C13—O12—H24	109.5	C2—C3—C4	110.8 (4)
C3—O3—H6	109.5	C4—C3—H5	109.5
C12—O11—H22	109.5	O16—C13—C14	110.3 (4)
C9—O9—H16	109.5	O16—C13—H23	110.5
C11—O7—C7	113.3 (4)	O12—C13—O16	107.8 (4)
C15—O14—H28	109.5	O12—C13—C14	107.3 (4)
C10—O10—H18	109.5	O12—C13—H23	110.5
O19—C20—H35	110.8	C14—C13—H23	110.5
O19—C20—C21	110.0 (4)	O14—C15—C14	107.7 (4)
O19—C20—C19	108.7 (4)	O14—C15—H27	108.9
C21—C20—H35	110.8	O14—C15—C16	113.1 (4)
C19—C20—H35	110.8	C14—C15—H27	108.9
C19—C20—C21	105.6 (4)	C14—C15—C16	109.3 (4)
O8—C8—H13	109.2	C16—C15—H27	108.9
O8—C8—C7	109.8 (4)	O21—C22—C23	109.3 (4)
O8—C8—C9	111.1 (4)	O21—C22—C21	109.8 (4)
C7—C8—H13	109.2	O21—C22—H39	109.1
C7—C8—C9	108.3 (4)	C23—C22—C21	110.5 (4)
C9—C8—H13	109.2	C23—C22—H39	109.1
O22—C24—H42	109.8	C21—C22—H39	109.1
O22—C24—H43	109.8	O2—C2—C1	110.7 (4)
O22—C24—C23	109.2 (4)	O2—C2—C3	111.5 (4)

H42—C24—H43	108.3	O2—C2—H3	107.9
C23—C24—H42	109.8	C1—C2—H3	107.9
C23—C24—H43	109.8	C3—C2—C1	110.9 (4)
O5—C1—H1	108.2	C3—C2—H3	107.9
O5—C1—C2	109.3 (4)	O4—C4—C5	105.4 (4)
O1—C1—O5	112.8 (4)	O4—C4—C3	111.3 (4)
O1—C1—H1	108.2	O4—C4—H7	109.8
O1—C1—C2	109.9 (4)	C5—C4—C3	110.6 (4)
C2—C1—H1	108.2	C5—C4—H7	109.8
O18—C23—C24	105.9 (4)	C3—C4—H7	109.8
O18—C23—H41	109.3	O17—C18—C17	111.6 (4)
O18—C23—C22	110.8 (4)	O17—C18—H31	109.3
C24—C23—H41	109.3	O17—C18—H32	109.3
C24—C23—C22	112.2 (4)	C17—C18—H31	109.3
C22—C23—H41	109.3	C17—C18—H32	109.3
O20—C21—C20	113.6 (4)	H31—C18—H32	108.0
O20—C21—H37	107.0	O15—C16—C17	105.9 (4)
O20—C21—C22	110.6 (4)	O15—C16—C15	111.4 (4)
C20—C21—H37	107.0	O15—C16—H29	109.4
C22—C21—C20	111.2 (4)	C17—C16—H29	109.4
C22—C21—H37	107.0	C15—C16—C17	111.2 (4)
O15—C19—O18	106.9 (4)	C15—C16—H29	109.4
O15—C19—C20	111.2 (4)	O9—C9—C8	111.2 (4)
O15—C19—H34	110.2	O9—C9—H15	107.8
O18—C19—C20	108.1 (4)	O9—C9—C10	111.3 (4)
O18—C19—H34	110.2	C8—C9—H15	107.8
C20—C19—H34	110.2	C10—C9—C8	110.6 (4)
O6—C6—H9	109.4	C10—C9—H15	107.8
O6—C6—H10	109.4	O10—C10—C9	107.4 (4)
O6—C6—C5	111.2 (4)	O10—C10—H17	109.7
H9—C6—H10	108.0	O10—C10—C11	111.6 (5)
C5—C6—H9	109.4	C9—C10—H17	109.7
C5—C6—H10	109.4	C9—C10—C11	108.7 (4)
O13—C14—H25	107.4	C11—C10—H17	109.7
O13—C14—C13	110.1 (4)	O7—C11—C10	110.7 (4)
O13—C14—C15	114.1 (4)	O7—C11—H19	109.3
C13—C14—H25	107.4	O7—C11—C12	106.1 (5)
C15—C14—H25	107.4	C10—C11—H19	109.3
C15—C14—C13	110.1 (4)	C12—C11—C10	112.0 (4)
O16—C17—H30	109.5	C12—C11—H19	109.3
O16—C17—C18	106.4 (4)	O11—C12—C11	113.3 (5)
O16—C17—C16	110.0 (4)	O11—C12—H20	108.9
C18—C17—H30	109.5	O11—C12—H21	108.9
C18—C17—C16	111.9 (4)	C11—C12—H20	108.9
C16—C17—H30	109.5	C11—C12—H21	108.9
O4—C7—O7	107.4 (4)	H20—C12—H21	107.7